Geographic boundary of the "Pacific Anomaly" and its geometry and transitional structure in the north

Yumei He[1] and Lianxing Wen[2,3]

Received 9 May 2012; revised 3 August 2012; accepted 6 August 2012; published 22 September 2012.

[1] We determine the geographical boundary and average shear velocity structure of the Pacific Anomaly at the base of the mantle based on travel time analysis of ScSH-SH and ScS2 (ScSScS)-SS phases and waveform modeling results. We further constrain the detailed geometry of the northern Anomaly around (20°N, −170°E) and its transition to the surrounding high velocity region along three perpendicular cross sections on the basis of forward waveform modeling of the observed direct S and ScS phases. The observed differential travel-time residuals and waveform modeling results allow the whole geographic boundary of the Anomaly to be delineated and the area of the base of the Anomaly is estimated to be 1.9×10^7 km^2. The maximum shear velocity perturbation inside the Anomaly reaches −5% in the lowermost 500 km of the mantle. Waveform analysis suggests that the northern Anomaly reaches 450 km above the CMB with both steeply and shallowly dipping edges and its basal layer extends beneath the surrounding mantle with the degree of extension changing rapidly across a small distance. The inferred characteristics of the Anomaly support the previous suggestion that the Pacific Anomaly represents a chemical anomaly. However, unlike the inferred features of the African Anomaly pointing to an ancient compositionally distinct and geologically stable anomaly, the existence of several separated piles extending into the mid-lower mantle, the complex morphology of the piles with both steeply and shallowly dipping edges and the presence of many ultra-low velocity zones at its base suggest that the Pacific Anomaly likely possesses varying intrinsic compositions and exhibits complex interaction with the surrounding mantle.

Citation: He, Y., and L. Wen (2012), Geographic boundary of the "Pacific Anomaly" and its geometry and transitional structure in the north, *J. Geophys. Res.*, *117*, B09308, doi:10.1029/2012JB009436.

1. Introduction

[2] In the last two decades, tomographic inversion, travel time analysis and waveform modeling studies have revealed various features of a large low shear velocity province at the base of the mantle beneath the Pacific Ocean (the Pacific Anomaly). Seismic studies suggest that the Pacific Anomaly occupies a broad area (about 10,000 km across) at the base of the mantle [e.g., *Mégnin and Romanowicz*, 2000; *Masters et al.*, 2000; *Grand*, 2002; *Trampert et al.*, 2004; *Houser et al.*, 2008; *Kustowski et al.*, 2008; *Panning et al.*, 2010; *Simmons et al.*, 2010; *Ritsema et al.*, 2011], with many ultra-low velocity zones (ULVZ) situated at the core-mantle boundary (CMB) beneath western Pacific for both P and S waves [e.g., *Garnero and Helmberger*, 1996; *Wen and Helmberger*, 1998a, 1998b; *Vidale and Hedlin*, 1998; *Rost and Revenaugh*, 2003; *Thorne and Garnero*, 2004; *McNamara et al.*, 2010], complex structures beneath the central Pacific [*Mori and Helmberger*, 1995; *Bréger and Romanowicz*, 1998; *Russell et al.*, 2001; *Wen*, 2002; *Avants et al.*, 2006; *Lay*, 2006; *Ohta et al.*, 2008], sharp edges [*To et al.*, 2005; *Ford et al.*, 2006; *He and Wen*, 2009], low shear velocity anticorrelated with high bulk sound velocity [*Masters et al.*, 2000], and possibly high density [*Ishii and Tromp*, 1999; *Romanowicz*, 2001]. Those seismic results suggest the Pacific Anomaly is chemically distinct from the ambient mantle. Based on these seismic results, various geodynamical models have been proposed to explain the origin, evolution and dynamic process of the Anomaly [*McNamara and Zhong*, 2004; *Schubert et al.*, 2004; *McNamara and Zhong*, 2005; *Tan and Gurnis*, 2007].

[3] In our previous studies, we have mapped out the northwest portion of the geographical boundary of the Pacific Anomaly beneath the western Pacific Ocean and studied the detailed structural features and shear velocity

[1]Key Laboratory of the Earth's Deep Interior, Institute of Geology and Geophysics, Chinese Academy of Sciences, Beijing, China.
[2]Department of Geosciences, State University of New York at Stony Brook, Stony Brook, New York, USA.
[3]School of Earth and Space Sciences, University of Science and Technology of China, Hefei, China.

Corresponding author: Y. He, Key Laboratory of the Earth's Deep Interior, Institute of Geology and Geophysics, Chinese Academy of Sciences, Beijing 100029, China. (ymhe@mail.igcas.ac.cn)

0148-0227/12/2012JB009436

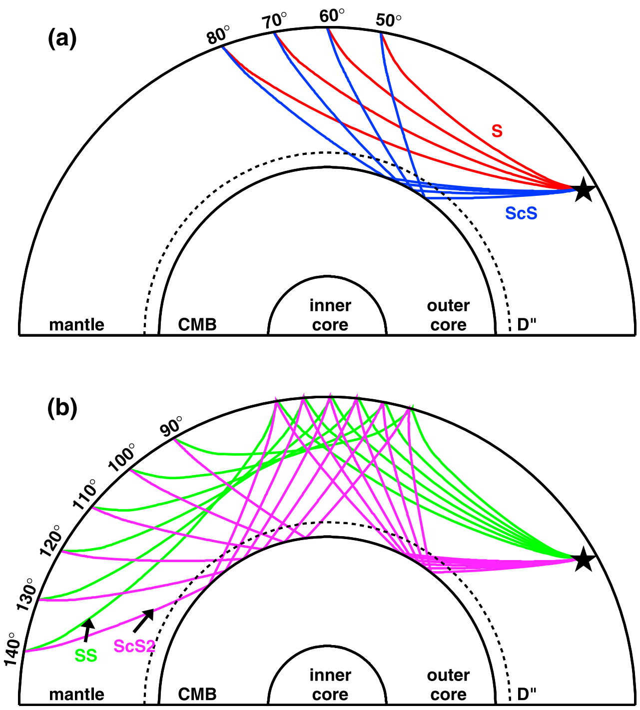

Figure 1. (a) Raypaths of direct S (red lines) and ScS (blue lines) at epicentral distances from 50° to 80°. (b) SS (green lines) and ScS2 (purple lines) at epicentral distances from 90° to 140°. These raypaths are calculated on the basis of PREM and a source depth of 300 km.

structures of the Anomaly along a cross-section from eastern Eurasia to southern South America [*He et al.*, 2006; *He and Wen*, 2009]. The seismic observations suggested that the Pacific Anomaly consists of at least two separated portions with a 740-km wide gap between them. Waveform modeling further suggested a high-velocity layer adjacent to the northwestern edge of the Anomaly. In this paper, we try to improve on the previous work on three aspects: 1) map out the whole geographic boundary and average shear-velocity perturbations of the Pacific Anomaly at the base of the mantle based on ScS-SH and ScS2-SS differential travel-time analysis and waveform modeling results, 2) determine the detailed geometric feature and shear-velocity structure of northern Anomaly in the mid-lower mantle and 3) constrain the transition of the northern Anomaly to the surrounding mantle based on waveform modeling. We also discuss the origin and dynamic process of the Anomaly in the context of the seismic results. We show seismic data in Section 2, present constraints on the whole geographic boundary, the geometries and detailed shear-velocity structures of the northern Anomaly and the transition from the northern Anomaly to the surrounding high velocity structure in Section 3, and discuss possible origins of the Anomaly based on the inferred seismic results and in comparison with the African Anomaly, another low velocity province in the lower mantle beneath Africa, in Section 4.

2. Seismic Data

[4] We focus our study area on a region near the CMB between −60°–40°N and 120°–285°E and deduce the whole geographic boundary of the Pacific Anomaly from ScS-SH and ScS2-SS differential travel-time residuals and waveform modeling results (Figure 1). Due to the limited station and event coverage, ScS2-SS differential travel times provide supplementary information to the area with poor ScS-SH sampling. We further constrain the geometries and velocity structures of the northern Anomaly and the transition from the northern Anomaly to the surrounding mantle based on waveform modeling of direct S and core-reflected ScS phases.

[5] We collect broadband tangential displacements of S and ScS phases recorded at a distance range between 45° and 85° for all the events occurring from 1994 to 2009, with a magnitude greater than 5.8 and the ScS bouncing points located at the CMB beneath the Pacific Ocean. Combining with the 619 ScS-S travel-time residuals we used in our previous study [*He et al.*, 2006], we choose 250 earthquakes and hand-pick a total of 1932 ScS-S travel-time residuals (Figure 2a and Data Set S1 in the auxiliary material).[1] Seismic data are collected from the China National Digital Seismographic Network (CNDSN), the F-net in Japan and the database of the Incorporated Research Institutions for Seismology (IRIS).

[6] We also collect travel-time residuals between ScS2 phase, an S phase bounced twice at the CMB, and SS phase, an S phase reflects off the Earth's surface once (Figure 1b). Seven earthquakes with 125 pairs of clear ScS2 and SS phases recorded at a distance range between 90° and 140° are selected to provide supplementary information inside the Anomaly where ScS-S residuals have sparse coverage (Data Set S2 in the auxiliary material). Those events occurred in the Tonga-Fiji subduction zone and south of New Zealand islands; the seismic data are recorded in North and South Americas (Figure 3a). The Hilbert transform is applied to the SS waveforms before we handpick the SS phase arrival times [*Choy and Richards*, 1975].

[7] We further use waveforms recorded on the Alaska Regional Network and the United States National Seismic Network for three events occurring in the Tonga subduction zone and Solomon Islands to constrain the detailed geometric features and seismic structures of the northern Anomaly and its transition to the surrounding high velocity region. The SH hybrid method [*Wen*, 2002] is applied to calculate synthetic seismograms.

[8] All data are deconvolved with their instrumental responses and bandpass-filtered from 0.008 to 1 Hz.

3. Geographic Boundary and Shear-Velocity Structure of the "Pacific Anomaly"

3.1. Geographic Boundary and Average Velocity Perturbations of the Base of the Anomaly

[9] Average velocity perturbations at the base of the Anomaly are estimated based on the ScS-S and ScS2-SS differential travel time residuals. The geographic boundary of the Pacific Anomaly is deduced based on waveform modeling results and the transition from the low-velocity to high-velocity perturbations along with possible errors in the inference of the geographic locations.

[1] Auxiliary material data sets are available at ftp://ftp.agu.org/apend/journal/2012jb009436. Other auxiliary material files are in the HTML. doi:10.1029/2012JB009436.

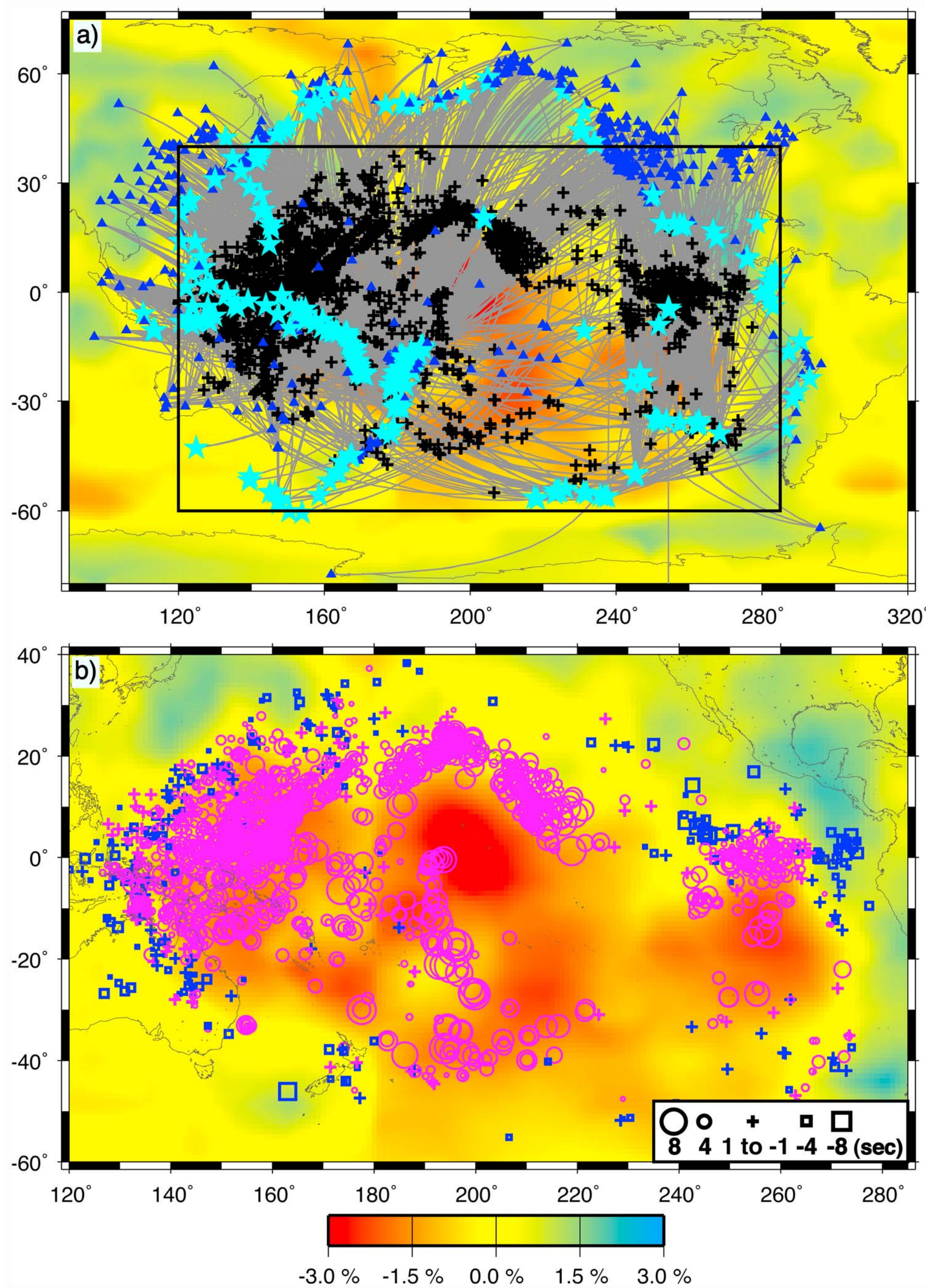

Figure 2. (a) The study region and ScS reflected points (black crosses) at the CMB, along with earthquakes (blue stars), seismic stations (deep blue triangles), and great circle paths (gray lines) of the seismic phases used in this study. The background is shear-velocity perturbations from a global shear-velocity tomographic model GyPSuM [*Simmons et al.*, 2010]. The rectangle box indicates a region where detailed ScS-S differential time residuals are presented in Figure 2b. (b) Observed ScS-S differential time residuals plotted at the ScS reflected points at the CMB, after corrected for the effects of the mantle heterogeneities 500 km above the CMB using a shear-velocity model GyPSuM [*Simmons et al.*, 2010]. The residuals smaller than -1 s are plotted as squares; those ranging from -1 to 1 s as crosses; and those larger than 1 s as circles. The sizes of the symbols are proportional to the magnitudes of the travel-time residuals.

[10] For ScS-S differential travel-time residuals, we remove the travel time contributions of the seismic heterogeneities 500 km above the CMB based on predictions of tomographic model GyPSuM [*Simmons et al.*, 2010]. The selection of the tomographic model and the cut-off depth for the corrections are based on following testing results. We test five tomographic models: GyPSuM [*Simmons et al.*, 2010], HMSL_S06 [*Houser et al.*, 2008], S362ANI [*Kustowski et al.*, 2008], S40RTS [*Ritsema et al.*, 2011] and TX2011 [*Grand*, 2002], and different cut-off depths (300 km, 400 km, 500 km and

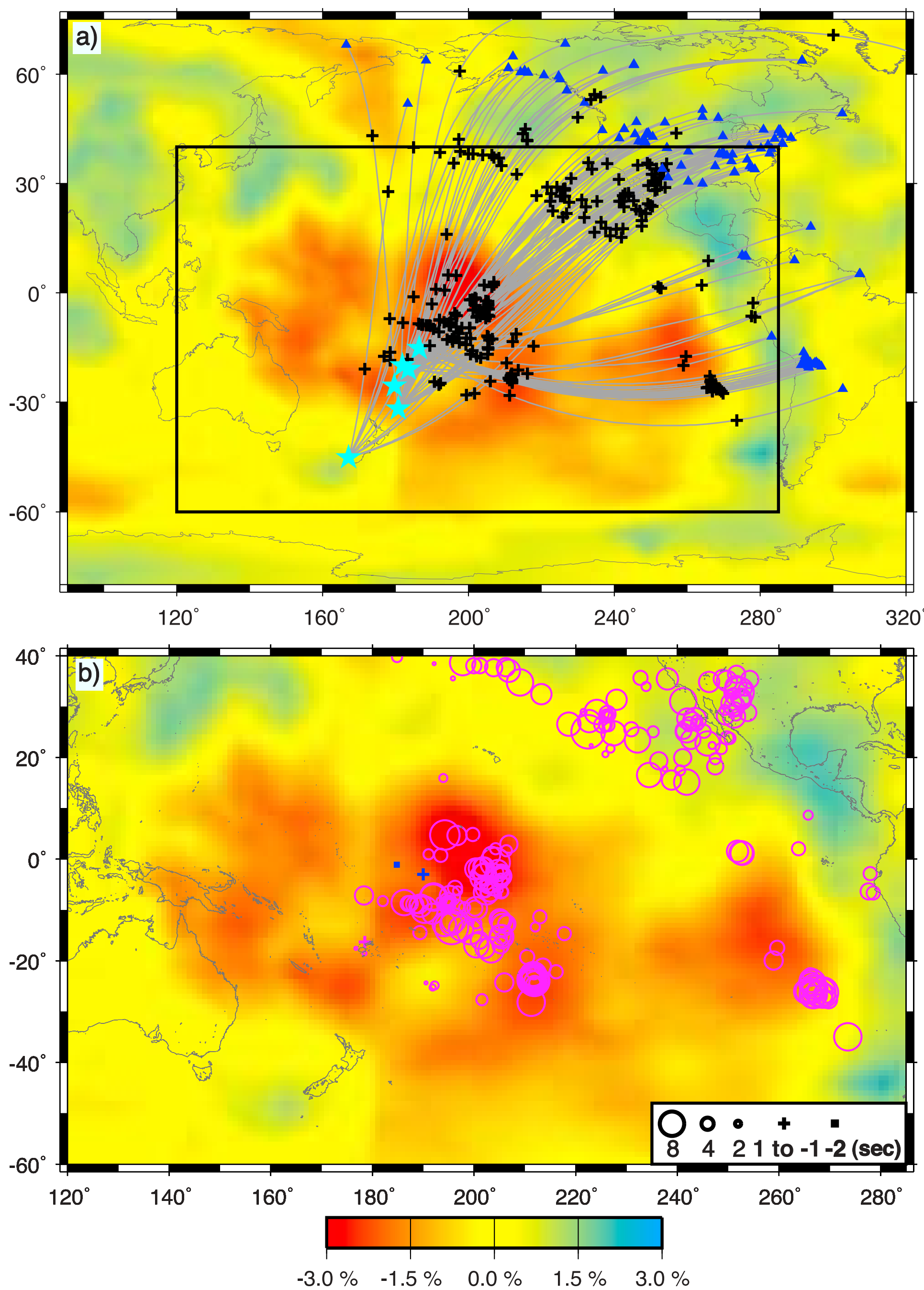

Figure 3. (a) The study region (black box) and ScS2 reflected points (black crosses) at the CMB, along with earthquakes (blue stars), seismic stations (deep blue triangles), and great circle paths (gray lines) of the seismic phases used in the study. (b) Observed ScS2-SS differential time residuals plotted at the ScS2 reflected points at the CMB, after corrected for the effects of the mantle heterogeneities 500 km above the CMB and outside the Anomaly, using a shear-velocity model GyPSuM [*Simmons et al.*, 2010].

600 km above the CMB) to explore the best way to correct the effects of the seismic heterogeneities outside the Pacific Anomaly. We use 500 km above the CMB as the cut-off depth for the corrections, because, for all the models tested, the correlations between the ScS travel-time residuals and the ScS-S differential travel-time residuals become the strongest when we use the cut-off depth of 500 km above the CMB. This probably reflects the fact that most of the low velocity anomalies beneath Pacific are situated in the lowermost 500 km of the mantle in the tomographic models. We choose model GyPSuM [*Simmons et al.*, 2010] for corrections as that model produces the best correlation between the corrected ScS travel time residuals and ScS-S differential travel time residuals (Table 1), although our results are affected little by the choice of a particular model for the corrections (Figure S1 in the auxiliary material). The corrected ScS-S differential travel

Table 1. Correlation Coefficients (CC)

	CC Between S and ScS-S	CC Between ScS and ScS-S	CC Between SS and ScS2-SS	CC Between ScS2 and ScS2-SS
Raw data	−0.11	0.76	−0.18	0.63
GyPSuM	−0.16	0.86	−0.13	0.83
HMSL_S06	−0.14	0.83	−0.17	0.76
S362ANI	−0.13	0.79	−0.09	0.83
S40RTS	−0.17	0.84	−0.13	0.86
TX2011	−0.15	0.86	−0.19	0.82

time residuals exhibit a large area of positive values beneath the Pacific Ocean surrounded by regions with neutral or negative values (Figure 2b). Variations of the ScS-S differential travel-time residuals inside the Anomaly are also observed. For example, around (−20°N, −170°E), travel time residuals increase rapidly from 2 to 3 s to 6–8 s within 200 km.

[11] The corrected ScS-S differential travel times could be caused either by a uniformly thick layer with lateral variations of shear velocity or by a layer with a uniform average velocity reduction with laterally varying thickness. In this study, as our main purpose is to map out the detailed geographic boundary of the Pacific Anomaly, we attribute the corrected ScS-S differential travel times to the seismic shear velocity variations in the lowermost 500 km of the mantle.

[12] The ScS2-SS differential travel times provide supplementary information in the lowermost mantle beneath eastern Pacific (Figure 3b). Since the ScS2 phase samples the CMB twice, we choose the data with one ScS leg sampling inside the Anomaly and another leg outside. We remove the travel time contributions of the seismic heterogeneities 500 km above the CMB and outside the Anomaly, based on the predictions of tomographic model GyPSuM [*Simmons et al.*, 2010]. We then attribute the corrected ScS2-SS differential travel-time residuals to the contributions of seismic structure in the lowermost 500 km of the mantle inside the Anomaly.

[13] Our correction is proved to be effective by comparing the relationships of the ScS2-SS differential travel-time residuals with SS and ScS2 travel-time residuals, before and after the corrections (Table 1 and Figure 4). Before the corrections, negative correlations are observed between the SS travel-time residuals and the ScS2-SS travel-time residuals. Strong scattering exists in both relationships (Figures 4a and 4b). After the corrections, the scattering is reduced in the SS travel-time residuals (Table 1 and Figure 4c) and the correlations between the ScS2 travel-time residuals and ScS2-SS differential travel-time residuals become strong (Figure 4d), indicating that our corrections indeed remove the effects of seismic heterogeneities 500 km above the CMB and outside the Pacific Anomaly.

[14] The maximal ScS2-SS differential travel-time residual reaches 11 s beneath northeastern Pacific. The ScS2-SS differential travel-time residuals also show relatively low values around (−20°N, −170°E).

[15] We estimate the magnitude of velocity perturbations by assuming that the corrected ScS-S and ScS2-SS differential travel times are caused by a lowermost 500 km thick layer with lateral variations of shear velocity (Figure 5). The magnitude of the ScS-S and ScS2-SS differential travel-time residuals suggests that the maximum shear velocity reduction of the Pacific Anomaly reaches −5% in the lowermost 500 km of the mantle. Small-scale velocity variations inside the Anomaly also exist. For example, around (−20°N, −170°E), the average velocity perturbations decrease rapidly from −1% to −2∼−3% within a 200-km distance range. We should however emphasize that the rapidly decrease of the velocity perturbations may also reflect rapid change of thickness of the Anomaly in the region.

[16] Waveform modeling analysis has constrained the exact locations of the geographic boundary of the Pacific Anomaly in a few regions (the portions of the contour represented by heavy lines in Figure 5). In particular, the northwestern boundary around (5°N, 155°E) was constrained in our previous study [*He and Wen*, 2009], while the northern boundary around (20°N, −170°E) is determined from extensive waveform modeling described in section 3.2. For the rest of the boundary, we derive it using the transitional boundary from positive travel-time residuals (low velocities) to negative or zero travel-time residuals (high or normal velocities) as reference and estimating its errors in various regions. The transition from low velocity perturbations to high or normal velocity perturbations surrounding the Pacific Anomaly can be clearly identified and mapped out, except in the region between Australia and New Zealand in southeast, and from −135°E to −120°E in the north due to relatively poor data sampling there (gray contour, Figure 5). Because the horizontal sampling distance of the ScS phase is large at the base of the mantle, the inference of the geographic boundary of the Anomaly based on the transition of the travel times alone would have uncertainties. The uncertainties would depend on data coverage, the direction of raypath with respect to the orientation of the Anomaly, and the seismic structure of the Anomaly in the lower mantle. In the regions with dense data coverage and seismic raypaths parallel to the boundary, the deduced boundaries based on the transition of travel time residuals would likely represent the real boundaries. This applies to the southern and southwestern boundaries (Figure S2 in the auxiliary material and Figure 5). For the regions with seismic raypaths sampling perpendicular to the boundary, waveform modeling analysis indicated that the actual geographic boundary may be further inward toward the Anomaly and the boundary location determined based the transition of the travel time residuals would have large uncertainties (for example, please see the northwestern boundary around (5°N, 155°E) in Figure 5). For the portion of the boundary determined based on the transition from the travel time residuals, we estimate uncertainties based on the seismic structure of the Anomaly in the lower mantle, the sampling direction of the raypath and the orientation of the Anomaly (Figure 5). The area of the base of the Pacific Anomaly is estimated to be 1.9×10^7 km^2, with an uncertainty of 15%.

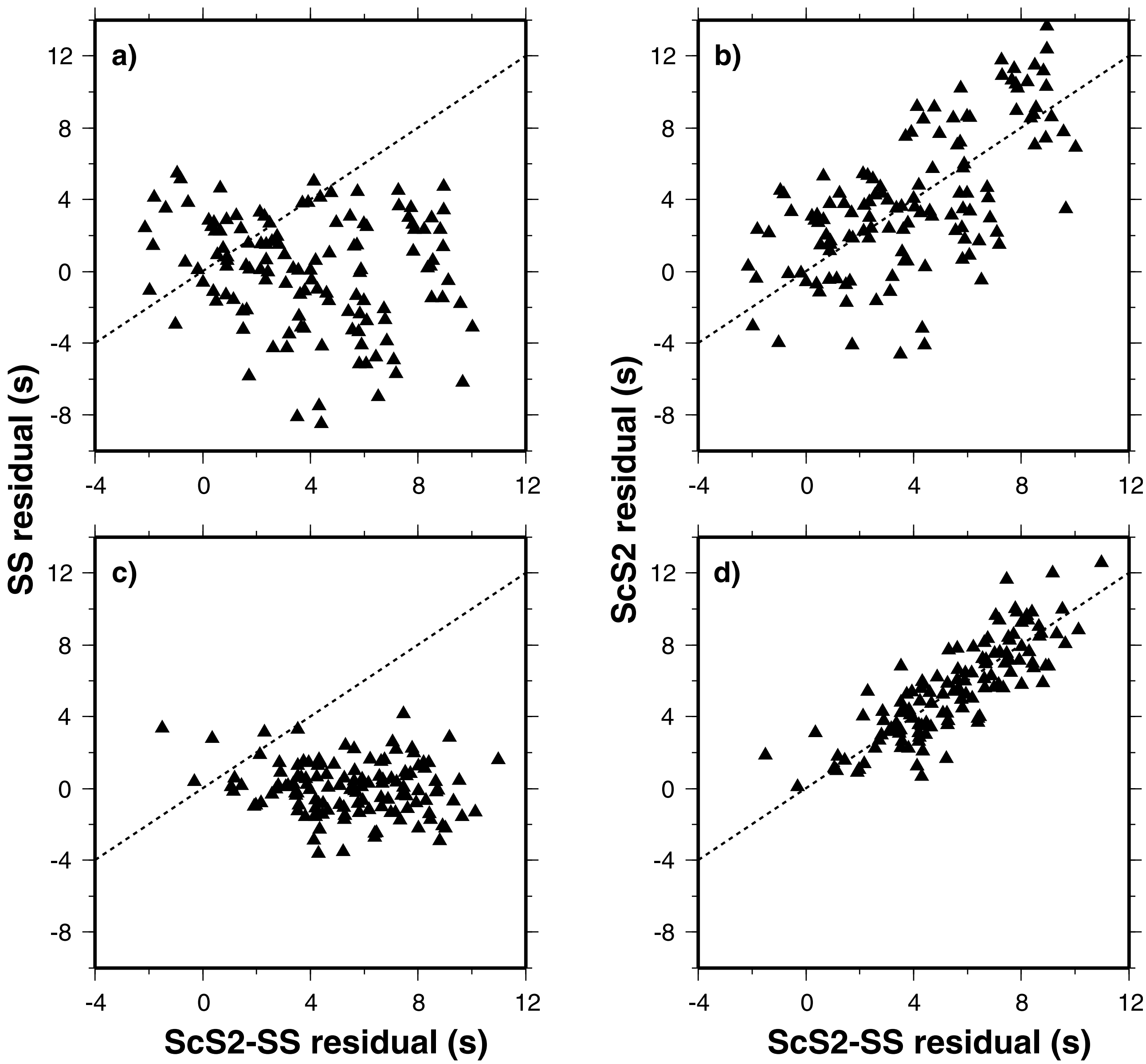

Figure 4. Relationship between observed SS travel-time residuals and ScS2-SS differential travel-time residuals (a) before and (c) after the corrections for the effects of the seismic heterogeneities 500 km above the CMB and outside the Pacific Anomaly based on a shear wave tomographic model GyPSuM [*Simmons et al.*, 2010]. Travel times are also corrected for array station statics. (b and d) Same as Figures 4a and 4c except for relationship between observed ScS2 travel-time residuals and ScS2-SS differential travel-time residuals. SS and ScS2 times are hand-picked from the seismograms. The Hilbert transform is applied to the SS waveforms before their times are picked. The dashed lines have a slope of 1 and intercept at (0, 0).

3.2. Detailed Features and Transitional Structures of the Northern Anomaly

[17] To further constrain the geometric feature and velocity structure of the northern Pacific Anomaly and the nature of the transition from the northern Anomaly to the surrounding high-velocity region, we select 3 events with their raypaths sampling the northern boundary of the Anomaly along near perpendicular cross-sections for waveform modeling (Figure 6 and Table 2). Event 2003/06/12 occurred in Solomon Islands and was recorded in North America. The raypaths of S and ScS phases are subparallel to the northern boundary. The tangential displacements of the event can be divided into two groups with one sampling inside the Pacific Anomaly and the other outside the Anomaly. Events 2003/07/27 and 2006/02/26 occurred in the Tonga-Fiji subduction zone and were recorded in Alaska. The raypaths of S and ScS phases of these two events are perpendicular to the northern boundary and are adjacent to each other. For the data sampling inside the Anomaly, there is overlap of ScS bouncing points between events 2003/06/12, 2003/07/27 and 2006/02/26 (Figure 6). The seismic data of these events sample the boundary areas inside and outside the northern Anomaly from different directions, placing tight constraints

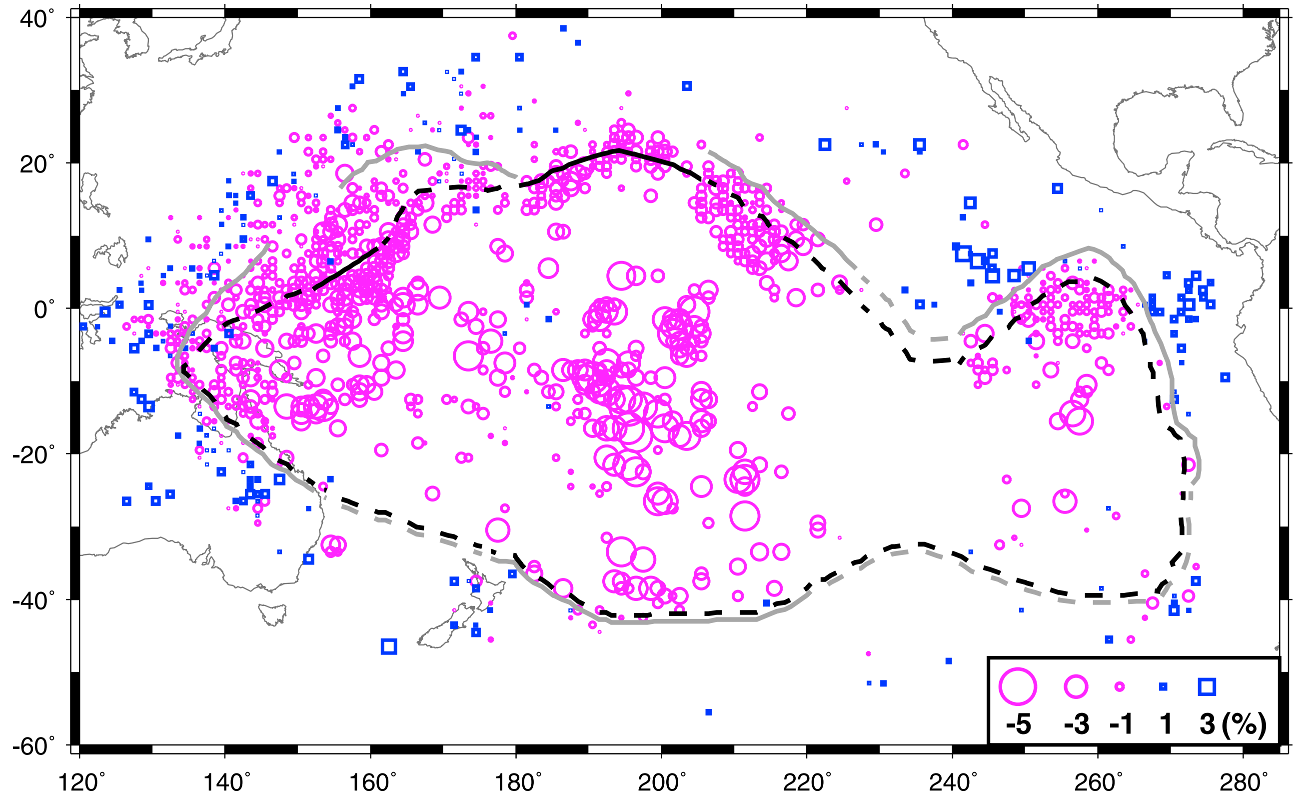

Figure 5. Average shear-velocity perturbations in the bottom 500 km of the mantle and the geographic boundary of the Pacific Anomaly at the base of the mantle (black contour). The transitional boundary from positive travel-time residuals (low velocities) to negative or zero travel-time residuals (high or normal velocities) is delineated as the possible outward locations of the geographic boundary of the Pacific Anomaly (gray contour). The velocity perturbations are inferred from the corrected travel-time residuals of ScS-S in Figure 2b and ScS2-SS in Figure 3b. Negative velocity perturbations are plotted as circles, and positive velocity perturbations as squares. The sizes of the symbols are proportional to the magnitudes of velocity perturbations. The shear-velocity perturbations are averaged over 1 × 1 grids. The black contour marks the geographic boundary determined from the velocity perturbations and detailed waveform modeling, with the dashed portion being uncertain.

on the geometries and velocity structures of the northern Anomaly as well as the detailed transitional structure from the northern boundary to the surrounding mantle.

[18] The tangential displacements of event 2003/06/12 exhibit very different waveform characteristics between those sampling inside and outside the Anomaly at a similar distance range (88°–98°) (Figures 7 and 8). The seismic waves sample inside the Anomaly in an azimuthal range from 50° to 60° and exhibit a clear SH phase followed by a discernible ScS phase up to a distance of 97° (Figure 7a). The SH phases show a near-constant travel time delay of 2.5 s with respect to the predictions based on PREM [*Dziewonski and Anderson*, 1981]. The ScS phase has amplitudes comparable to the direct SH waves and exhibits travel time delays of 5.5 s∼6.5 s. On the other hand, for the seismic data sampling outside the Anomaly in an azimuthal range from 40° to 50°, no discernible ScS phases are observed at the distance range smaller than 90° (Figure 8a). The travel time delays of SH phases decrease from 2.0 s at 87.5° to 0 s at 91°, and then linearly increase to ∼3.5 s from 91° to 98°. There exist two strong phases immediately before and after the SH phases from 91° to 98°. These phases exhibit same polarity and comparable amplitudes as the direct SH phases. The anomalous phase (labeled Scd) ahead of the SH phase exhibits normal SH arrival times as predicted by PREM, while the phase following the SH phase (labeled Su) has travel time delays increasing from 0 s at 91° to ∼10 s at 98° (Figure 8a).

[19] The waveform complexities of event 2003/06/12 are markedly different between the two groups of the observations. The different complexities are most likely caused by the laterally varying seismic heterogeneities in the lowermost mantle, as they cannot be explained by other factors such as mislocation of the earthquake, complexities of source time function and the seismic heterogeneities in the source-side mantle. Mislocation of the earthquake and a complex source would result in a uniform travel time delay and similar waveform complexities across the stations. Two groups of the data have slightly different azimuth ranges of (40°–50°) and (50°–60°), and their raypaths are close at the source-side of the mantle, therefore the different complexities cannot be caused by the source-side seismic heterogeneities. Near-station effects and the upper mantle structure beneath North

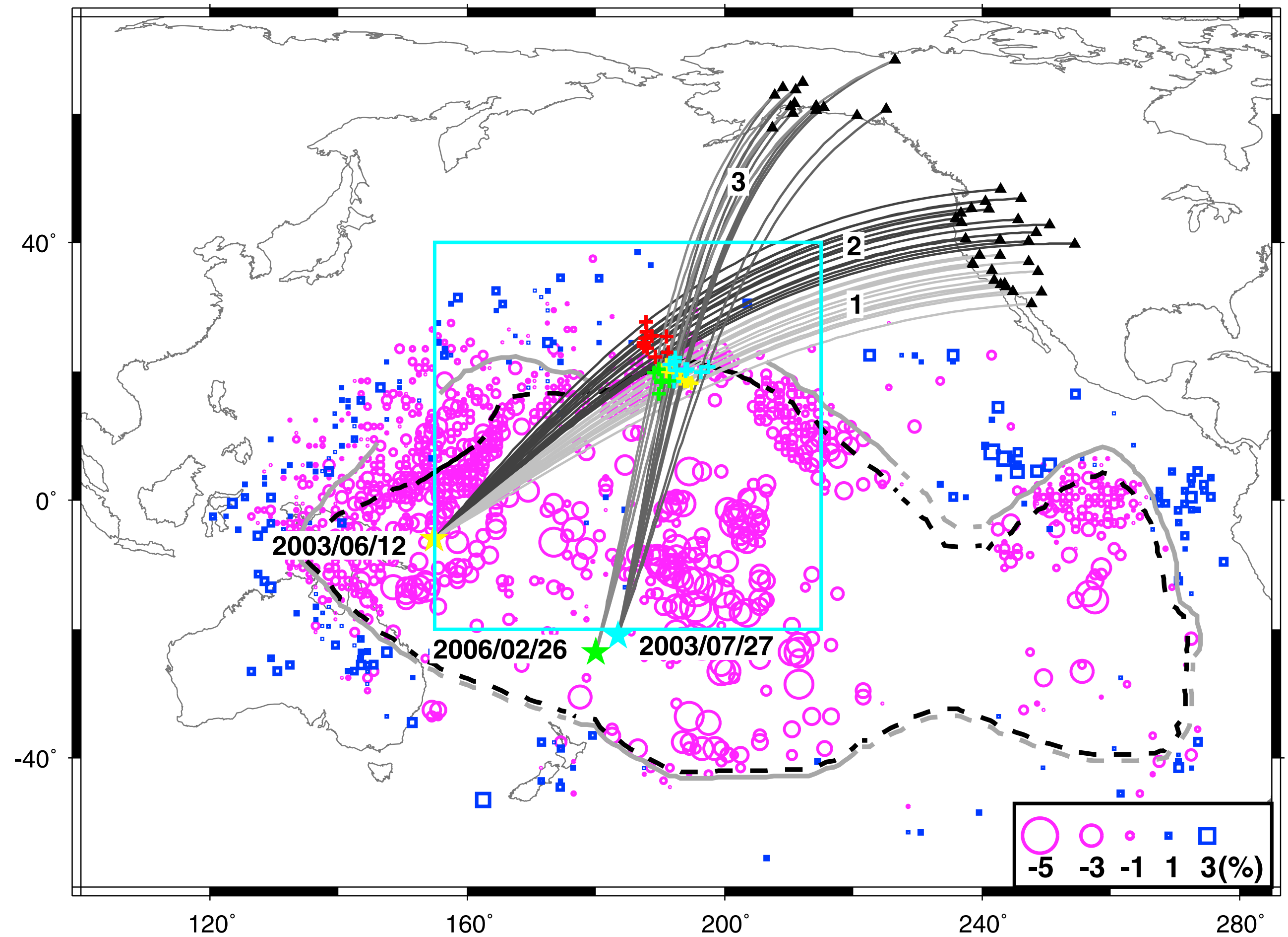

Figure 6. Selected 2-D cross-sections 1–3, ScS reflected points (crosses) at the CMB, along with earthquakes (stars), seismic stations (triangles), and great circle paths (gray lines), for earthquakes 2003/06/12, 2003/07/27, and 2006/02/26 whose waveforms are used to constrain the detailed seismic structures of the northern edge of the Anomaly. The average velocity perturbations and the geographic boundary (black and gray bold and dashed contours) deduced in this study (Figure 5) are also plotted as background. The rectangle box indicates a region where geometries and exact locations of the three cross-sections of the Pacific Anomaly are presented in Figure 11.

America appear to contribute little to the complexities across the stations as well, because the recordings at the same stations for one earthquake occurring in Hawaiian Islands show simple waveforms. Moreover, the observations from an earthquake in the Tonga-Fiji subduction zone to Alaska (Figures 6 and 9), which sample the same CMB region inside the Anomaly but different parts of the mid-lower mantle, show similar travel time behaviors for the S and ScS phases, confirming that the complexities observed in the North America are caused by anomalous seismic structures in the lowermost mantle.

[20] For records sampling inside the Anomaly (Figure 7a), the direct S phases show a travel-time delay of 2.5 s at 88.5°, indicating that the northern Pacific Anomaly extends more than 350 km above the CMB. The observed near-constant travel-time delays of 2.5 s from 88.5° to 97° also suggest the Anomaly has a steeply dipping edge along this sampling direction. The observed slowness of the ScS phases and the travel time delay of SH waves can be best explained by a 2D model with a thickness of 450 km, a steeply dipping edge and a basal layer extending beneath the surrounding high velocity region (Figure 7b). The velocity structure varies from −3% at the top to −3.5% at 40 km above the CMB and an average shear-velocity reduction of −5% in the bottom 40 km of the mantle. The high velocity structure has a velocity jump of 2% at 220 km above the CMB. The geometry of the Pacific Anomaly is well constrained by the travel time delays and relative amplitudes of SH and ScS phases, although there is a trade-off between the inferred thickness of the Anomaly in the mid-lower mantle and its exact geographic location. A thinner anomaly locating slightly east or a thicker anomaly locating slightly west could also reasonably explain the data. The acceptable thickness of the Anomaly along this section is in the range from 400 km to 500 km.

[21] The anomalous observations sampling outside the Anomaly (Figure 8a) are likely caused by 2D effects, since they sample across a certain azimuth (Figure 6) and show a distance dependence of the waveforms (Figure 8a). In fact, the observations can be well explained by a simple 1D model

Table 2. Events List[a]

Event	Origin Time	Latitude (°N)	Longitude (°E)	Depth (km)	Time Corrections (s)
2003/06/12	2003.163.08.59.20	−5.99(−5.99)	154.76(154.86)	186(176)	0.5
2003/07/27	2003.208.02.04.11	−21.08(−20.98)	−176.59(−176.59)	213(206)	2.0
2006/02/26	2006.057.03.08.27	−23.61(−23.51)	−179.99(−179.99)	535(520)	0.5

[a]Values in parentheses are relocated latitude, longitude, and depth.

with a high-velocity layer in the lowermost mantle (Figure 8), suggesting that the observations are mainly influenced by the high velocity structure surrounding the Pacific Anomaly. A model that has a velocity jump of 2.0% at 240 km above the CMB can explain the observations between 87° and 90°, and the emergence of the Scd phases before the SH phases after 91° (Figures 8a and 8b). The anomalous phases after SH phases (labeled Su) can be explained by S wave refractions in the low velocity area with a thickness of 460 km and a velocity reduction of −1% located above the bottom high velocity layer (Figure 8c). A thickness of the low velocity layer smaller than 400 km would not generate Su phases with proper travel time delays. A velocity reduction greater than −1.2% would produce too strong an Su phase and too large travel time delays of SH phases, to fit the observations. A velocity reduction lower than −0.8%, on the other hand, would produce too weak an Su phase to fit the data.

[22] The seismic waves propagating from the Tonga-Fiji subduction zone to Alaska show varying waveforms at close distances (Figures 6, 9, and 10). The seismic data of events 2003/07/27 and 2006/02/26 sample the northern boundary of the Pacific Anomaly perpendicularly within an azimuthal range of 6° (Figure 6). The tangential displacements of event 2003/07/27 exhibit clear SH and ScS phases at a distance range of 81°–94° (Figure 9a). The SH phase shows no obvious travel time delays up to a distance of 94°. The ScS phase has travel time delays slightly decreasing from 5.5 s at 81° to 5 s at 94°. Event 2006/02/26 is located southwest of event 2003/07/27 (Figure 6). The SH phase shows no travel time delays up to a distance of 97°, while the ScS phase has travel time delays of 4.5 s from 84° to 91°. Despite the close proximity of ScS bouncing points between events 2003/07/27 and 2006/02/26, the ScS waveforms varied from simple pulses for event 2003/07/27 (Figure 9a) to multiple pulses for event 2006/02/26 (Figure 10a).

[23] The travel time delays of events 2003/07/27 and 2006/02/26 and anomalous phases of 2006/02/26 are most likely caused by anomalous seismic structure in the lowermost mantle. The ScS travel time delays cannot be caused by mislocation of the earthquakes, complexities of earthquake

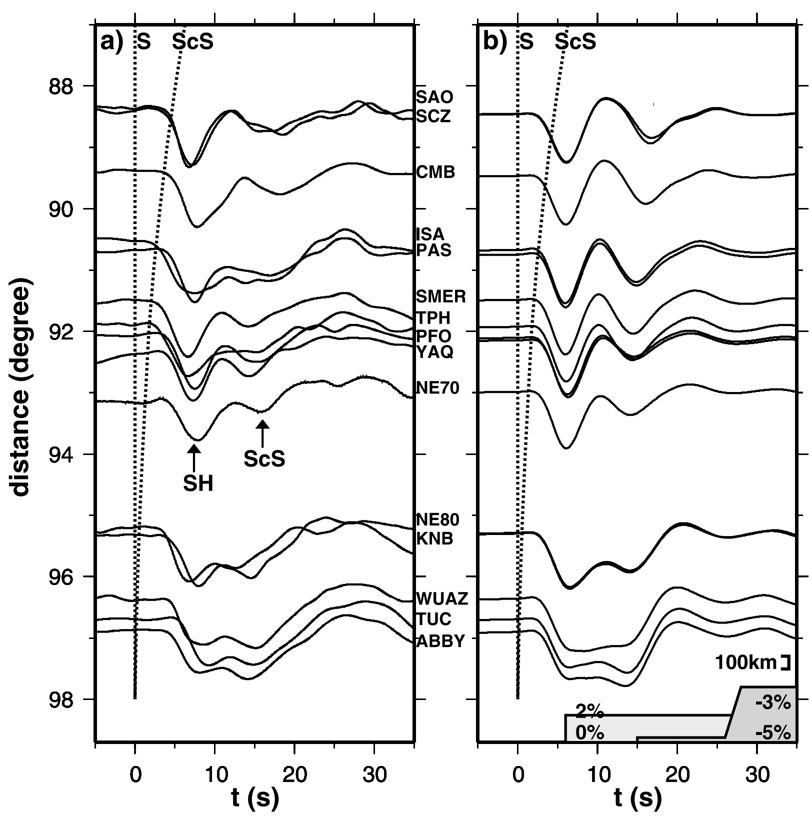

Figure 7. (a) Observed tangential displacements for event 2003/06/12 for the cross section sampling inside the Pacific Anomaly (cross section 1 in Figure 6). (b) Synthetics calculated based on a 2D model shown in the bottom of the panel. The theoretical arrivals of SH and ScS phases based on PREM are plotted in dashed lines in Figures 7a and 7b, and the observed phases are labeled by arrows in Figure 7a.

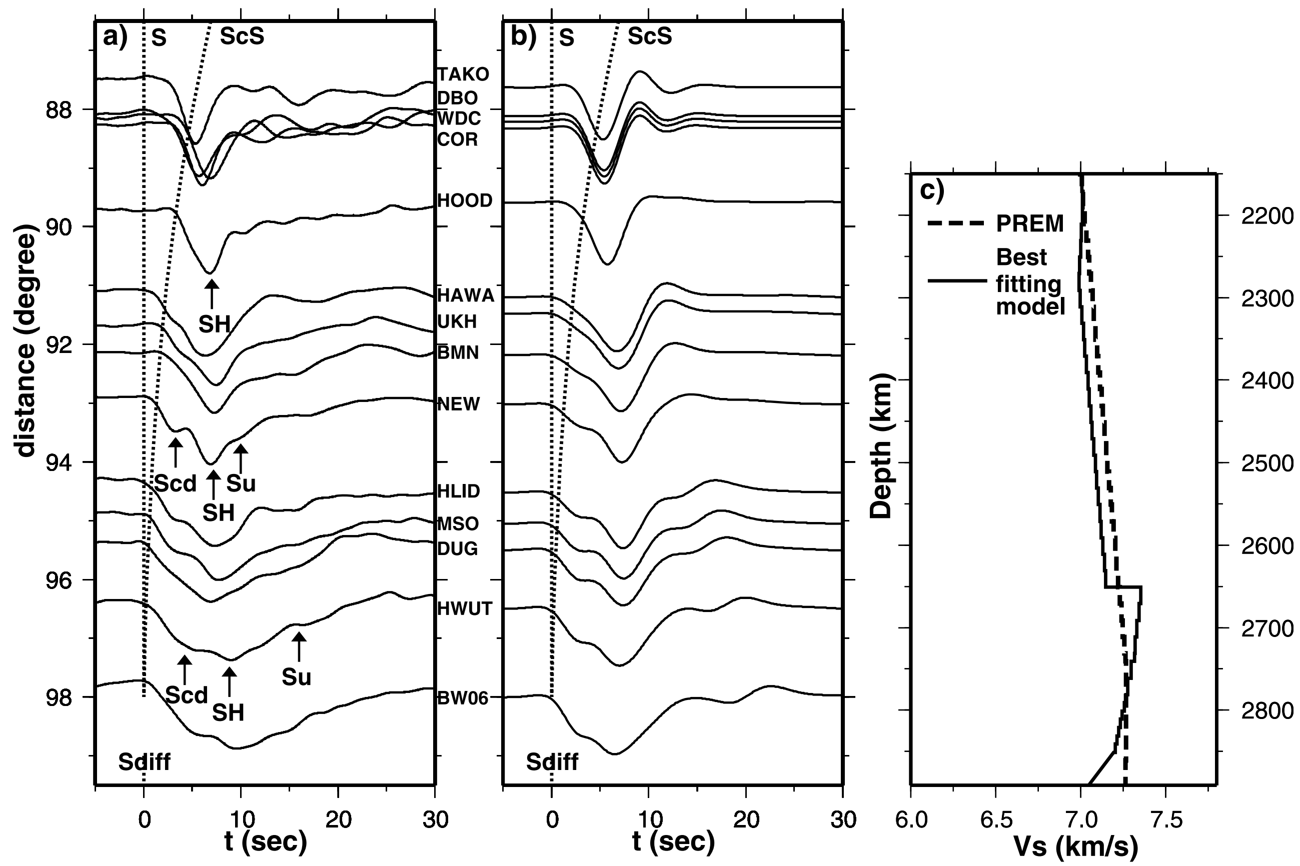

Figure 8. (a) Observed tangential displacements for event 2003/06/12 for the cross section sampling outside the Pacific Anomaly (cross section 2 in Figure 6). (b) Synthetics calculated based on the one-dimensional (1D) model shown in Figure 8c. (c) The best fitting 1D shear velocity model along with PREM. The theoretical arrivals of SH and ScS phases based on PREM are plotted in dashed lines in Figures 8a and 8b. The observed Scd, SH and Su phases are indicated by arrows in Figure 8a.

source, or seismic heterogeneities in the source-side mantle, as these factors would generate similar travel time delays for both S and ScS phases. Those two events are recorded at the same stations in Alaska with different waveform patterns, which also exclude the seismic heterogeneities in the receiver-side mantle as the causes.

[24] Since both SH phases of these two events show no travel time delays up to a distance of 97°, we do not have a tight constraint on the thickness of the Anomaly. A low-velocity anomaly in the lower mantle with a thickness of 300 km or 500 km with varied widths would generate synthetics that fit the data equally well. However, considering the fact that these two events sampling lowermost mantle close to each other and the low velocity anomaly nearby has a thickness of 450 km (Figures 6 and 7), we also explain the observations with a low-velocity anomaly in the lower mantle with a same thickness of 450 km. In this case, a high velocity structure is also required to be adjacent to the low-velocity anomaly to cancel the travel time delays of SH phases generated by the low-velocity anomaly. Though these two events show very different waveforms, the observations can be well explained by similar models with a low-velocity anomaly in the lower mantle with a thickness of 450 km and a shallowly dipping edge extending beneath the surrounding high velocity region. A model with steeply dipping edges or without the surrounding high velocity structure cannot produce synthetics that fit the observations of event 2006/02/26, especially at station INK (Figure 10a). The velocity structure varies from −3% at the top to −3.5% at 60 km above the CMB, and an average shear-velocity reduction of −5% in the bottom 60 km of the mantle (Figures 9b, 10b, and 11). The high velocity structures have velocity jump of 2% at 220 km above the CMB, respectively. A longer basal layer beneath a high velocity structure generates multiple phases after the SH phase, resembling the multiple ScS phases of event 2006/02/26. The results are consistent with those deduced from the anomalous observations of event 2003/06/12 sampling inside and outside the Anomaly (Figures 7b, 8c, and 11).

[25] We have performed waveform modeling based on 2D wave propagation. The 3D effects on waveform complexities have been reported and studied for the seismic structures near the CMB [e.g., *Ni et al.*, 2005; *To and Romanowicz*, 2009; *Sun et al.*, 2009]. In this study, the waveform characteristics observed in each group of the stations exhibit clear change with epicentral distance, indicating that the waveforms are mainly affected by 2D heterogeneities. The

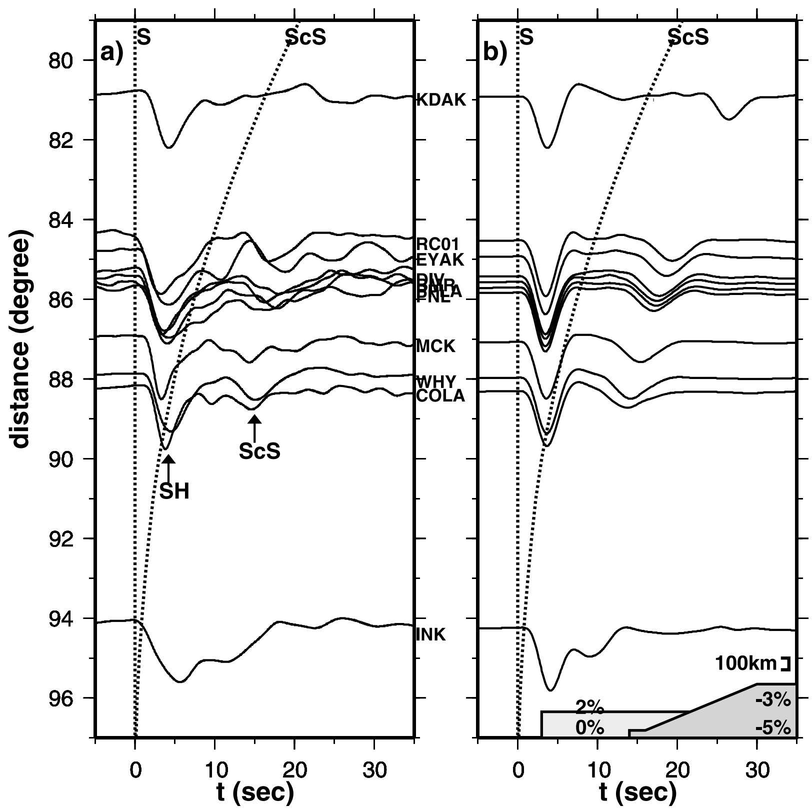

Figure 9. (a) Tangential displacement records for events 2003/07/27 for a cross section sampling perpendicular to the northern boundary of the Anomaly (cross section 3 in Figure 6). (b) Synthetics calculated based on a 2D model shown in the bottom of the panel. The theoretical arrivals of SH and ScS phases based on PREM are plotted in dashed lines in Figures 9a and 9b. The observed SH and ScS phases are indicated by arrows in Figure 9a.

validity of the 2D approximations is further supported by the similarities of the inferred 2D structures in different sections.

4. Discussions

[26] As two nearly antipodal large low-shear velocity provinces in the lowermost mantle, the Pacific Anomaly and the African Anomaly have similarities and differences. Both Anomalies occupy broad areas at the CMB (about 1.9×10^7 km^2 for the Pacific Anomaly and 1.8×10^7 km^2 for the African Anomaly [*Wang and Wen*, 2004]). Both have bulk sound velocity increase anticorrelated with shear velocity reduction [*Masters et al.*, 2000], sharp edges [*Wen et al.*, 2001; *Wen*, 2001; *To et al.*, 2005], shear velocity perturbations of -3% in the mid-lower mantle [*Ni and Helmberger*, 2003; *Wang and Wen*, 2007; *Sun et al.*, 2009; *He and Wen*, 2009], and possibly higher densities [*Ishii and Tromp*, 1999; *Romanowicz*, 2001]. However, the two Anomalies also exhibit different structural features and seismic characteristics. Travel time analysis and waveform modeling indicate that the African Anomaly is a single massive pile with sharp edges, reaches 1300 km above the CMB and exhibits a "bell-like" geometry in the mid-lower mantle [*Wang and Wen*, 2007]. Detailed waveform modeling revealed steeply dipping edges, rapid varying structures and a strong negative shear velocity gradient from -2% (top) to -9 to -12% (bottom) in the lowermost 300 km of the African Anomaly [*Wen et al.*, 2001; *Wen*, 2001, *Wang and Wen*, 2004]. Different from the African Anomaly, our studies indicate that the Pacific Anomaly consists of several piles with both shallowly and steeply dipping edges in the mid-lower mantle (Figure 12). Those piles extend at least 740 km above the CMB beneath northwestern Pacific and 450 km beneath northern Pacific. The geometric features of the base of the Pacific Anomaly are less clear and we are only able to constrain the average shear-velocity reduction in the bottom 40–100 km of the mantle to be -5%, but many ULVZs exist at the base of the mantle beneath western Pacific for both P and S waves [e.g., *Garnero and Helmberger*, 1996; *Wen and Helmberger*, 1998a, 1998b; *Vidale and Hedlin*, 1998; *Rost and Revenaugh*, 2003; *McNamara et al.*, 2010]. And, as this study shows, the basal low-velocity layer extends beneath the surrounding high velocity region at various degrees and the degree of extension changes rapidly across a small distance.

[27] The geometry and stability of a chemical anomaly are controlled by its intrinsic properties (including density, rheological structure and degree of enrichment of heat-producing elements) and its interaction with background mantle flow. The geometry and velocity features of the base of the African Anomaly clearly indicate that it represents a primordial chemical anomaly [*Wen et al.*, 2001; *Wen*, 2001] and its geometry in the mid-lower mantle suggests that the

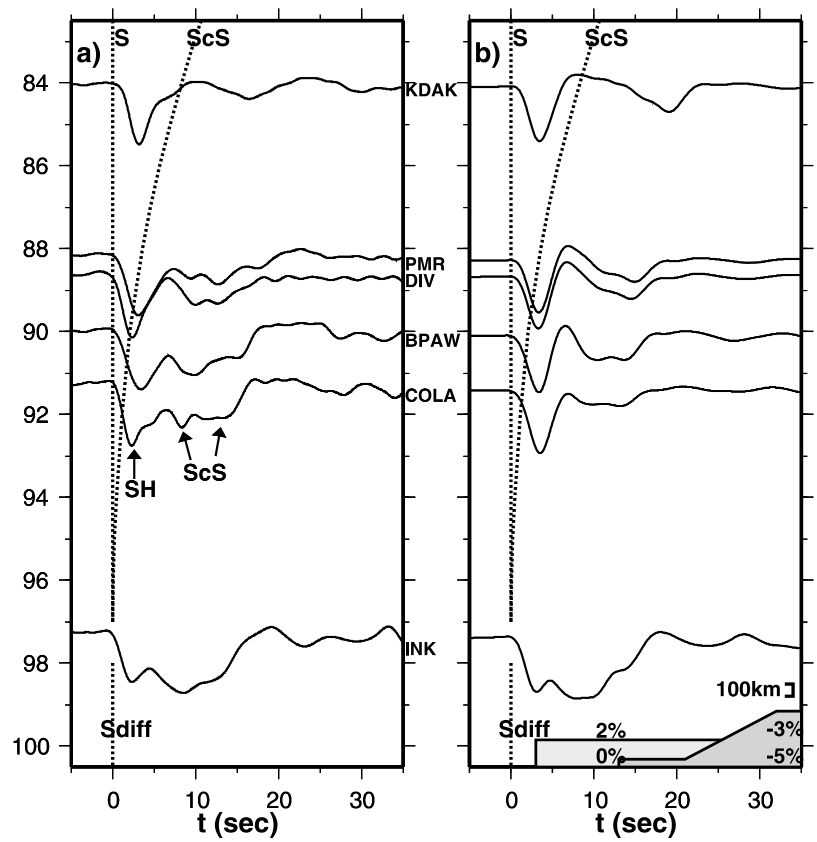

Figure 10. (a) Tangential displacement records for event 2006/02/26 for a cross section sampling perpendicular to the northern boundary of the Anomaly (cross section 3 in Figure 6). (b) Synthetics calculated based on a 2D model shown in the bottom of the panel. The theoretical arrivals of SH and ScS phases based on PREM are plotted in dashed lines in Figures 10a and 10b. The observed SH and ScS phases are indicated by arrows in Figure 10a.

Anomaly is geologically stable [*Wang and Wen*, 2007]. The inferred features that a basal layer of the Pacific Anomaly extends beneath the surrounding mantle is consistent with a geodynamical scenario that a dense, low-viscosity basal layer spreading out beneath the surrounding mantle, supporting the previous suggestions that the Pacific Anomaly represents a chemical anomaly. However, the lack of clear geometric features of the base of the Pacific Anomaly makes it difficult to pin down the origin of the Pacific Anomaly. The existence of at least two separated piles and the complex morphology of the piles with both steeply and shallowly dipping edges of the Pacific Anomaly in the mid-lower mantle suggest several possible origins for the Pacific Anomaly. While the shallowly dipping edges of the northern pile are consistent with those of a geologically stable chemical anomaly, the steep edges of the western pile are more consistent with those of a metastable thermo-chemical anomaly in some geodynamical simulations [*Tan and Gurnis*, 2007]. One possible explanation is that the two piles possess different intrinsic properties, leading to the development of different geometries as shown in some geodynamical modeling [*Tan and Gurnis*, 2007]. If the Pacific Anomaly represents a primordial anomaly, it may indicate that it is a collection of chemical anomalies produced by a complex event or a set of events in the early Earth's history that lead to varying intrinsic properties inside the Anomaly. On the other hand, the varying intrinsic properties could also have resulted from accumulation of subducted oceanic crust at various time periods of the Earth's plate tectonics history, or a mix of subducted oceanic crust with primordial materials. The existence of basal ULVZs may also reflect varying compositions within the Pacific Anomaly, as they may be caused by partial melt resulting from compositional changes [*Wen*, 2001; *Rost et al.*, 2005], iron-rich post-perovskite [*Mao et al.*, 2006] or presence of iron-rich (Mg, Fe)O in localized patches above the CMB [*Wicks et al.*, 2010].

[28] In addition, mantle flow patterns are likely very different beneath Africa and Pacific, and the difference of mantle flow between the two regions may also lead to the development of different characteristics of the two Anomalies [*McNamara and Zhong*, 2004]. The Pacific Anomaly is surrounded by the past subduction zone and some of the past subduction zone geographically falls inside the Anomaly [*Wen and Anderson*, 1995]. The past subduction in the Pacific could cut through the Pacific Anomaly, dividing it into several piles. The subduction could also enhance the return flow and entrainment in the region, shaping the geometry of the chemical piles in the mid-lower mantle. The transitional structures of the base of the Pacific Anomaly to the surrounding high-velocity region, that is, the basal low-velocity layer extends beneath the surrounding

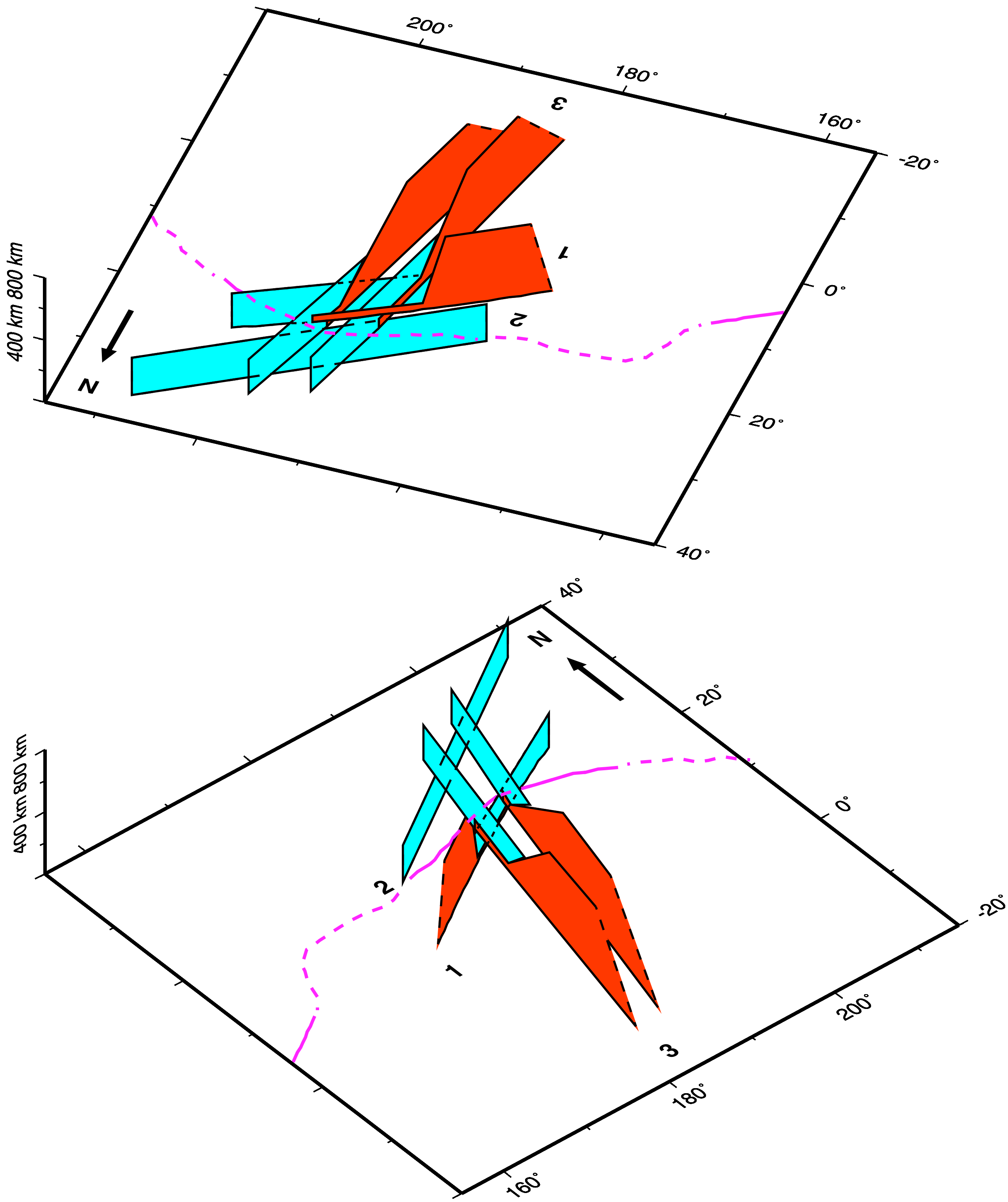

Figure 11. A three-dimensional view of the three constructed 2D model sections at the base of the mantle beneath northern Pacific viewed (top) from the azimuth of 340° and (bottom) from 220°. Three cross sections are labeled in accordance with those in Figure 6 and are from the waveform modeling results of Figure 7 (section 1), Figure 8 (section 2) and Figures 9 and 10 (section 3). The low velocity structures are shown in red and the surrounding high velocity regions in azure. The geographic boundary of the Pacific Anomaly deduced in Figure 5 are also plotted as purple lines.

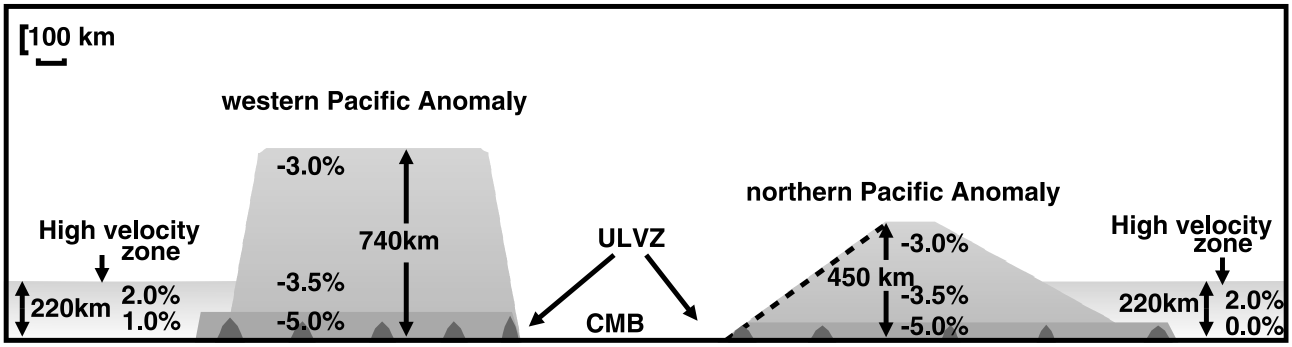

Figure 12. Schematic illustration of the inferred seismic features of the Pacific Anomaly. The Anomaly consists of two separated portions with the western portion reaching 740 km above the CMB with steeply dipping edges [*He and Wen*, 2009] and the northern portion reaching 450 km above the CMB with a shallowly dipping edge toward north (this study). A basal layer of thickness of 60–100 km extends beneath the surrounding northern and western high velocity regions. ULVZs are located at the base of the Anomaly. Shear-velocity perturbations are labeled for portions of the Anomaly and the surrounding regions. The dash line shows unresolved southward boundary of the northern portion of the Anomaly.

high velocity region at various degrees and the degree of extension changes rapidly across a small distance, indicate complex interaction of the Anomaly with the surrounding mantle flow [*McNamara et al.*, 2010]. Future geodynamical studies of mantle convection with realistic plate subduction history and varying intrinsic compositions of a chemical anomaly would better clarify the origin of the Pacific Anomaly and its interaction with the background mantle flow.

[29] Our inferred geographic boundary is similar to the −1% contour line of tomographic model GyPSuM (Figure S3 in the auxiliary material), except that our modeling results show that the northwestern boundary of the Anomaly locates more southeastward and the northern boundary of the Anomaly extends much northward. While various tomographic models give a similar shape of the geographic boundary of the Pacific Anomaly (Figure S3 in the auxiliary material), we believe a precisely determined geographic boundary of the Anomaly is of great importance. For example, the geographic boundaries of the Pacific and African Anomalies have been used to study the relationship with the locations of the surface hot spots [*Torsvik et al.*, 2006; *Burke et al.*, 2008]. These studies concluded that the hot spots are preferentially located near the edges of the two Anomalies. However, those conclusions were derived based on the geographic boundaries drawn from the tomographic models. While a precise geographic boundary of the African Anomaly determined from waveform modeling results [*Wang and Wen*, 2004] is used, all three long-live hot spots in the Indian and South Atlantic oceans (Tristan, Marion and Kerguelen) are actually geographically within the African Anomaly [*Wen*, 2006].

5. Conclusions

[30] We utilize the observed ScS-SH and ScS2-SS differential travel-time residuals and waveform modeling results to derive the whole geographic boundary of the Pacific Anomaly and average velocity structure in the lowermost 500 km of the mantle. We further use waveform analysis of the seismic data sampling the northern edge of the Anomaly to determine the detailed geometry of the northern Anomaly and its transition to the surrounding mantle. Waveform modeling results and travel time analysis of ScS-SH and ScS2-SS phases clearly define the whole geographic boundary of the Anomaly and the area of the base of the Anomaly is estimated to be 1.9×10^7 km^2, with an uncertainty of 15%. The maximum shear velocity perturbation inside the Anomaly reaches −5% in the lowermost 500 km of the mantle. Waveform analysis suggests that the northern Anomaly reaches 450 km above the CMB with both steeply and shallowly dipping edges, and its basal layers extend beneath the surrounding high velocity structure at various degrees and the degree of extension changes rapidly across a small distance. The inferred characteristics of the Anomaly imply that the Pacific Anomaly is a chemical anomaly. However, unlike the African Anomaly with its sharp and low-velocity basal layers pointing to a primordial compositional anomaly and its geometry in the mid-lower mantle suggesting a geologically stable anomaly, the existence of several separated piles in the mid-lower mantle, the complex morphology of the piles with both steeply and shallowly dipping edges, and many ULVZs at its base suggest that the Pacific Anomaly likely has varying intrinsic compositions and complex interaction with the surrounding mantle. The varying intrinsic compositions could be produced by a complex event or a set of events in the early Earth's history, or resulted from accumulation of subducted oceanic crust at various time periods of the Earth's plate tectonics history, or a mix of subducted oceanic crust with primordial materials. In addition, the past subduction could have divided the Pacific Anomaly into several piles and influenced the background mantle flow shaping the features of various portions of the Anomaly.

[31] **Acknowledgments.** We gratefully acknowledge the participants of the CNDSN, the F-net and the IRIS for their efforts in collecting the data. We thank Sebastian Rost and one anonymous reviewer for comments and suggestions that improved the paper significantly. Figures were made with the General Mapping Tools [*Wessel and Smith*, 1995]. This work was supported by the National Science Foundation of China (grants 41074059 and 40774041), Chinese Academy of Sciences and an NSF grant 0911319.

References

Avants, M., T. Lay, S. A. Russell, and E. J. Garnero (2006), Shear velocity variation within the D″ region beneath the central Pacific, *J. Geophys. Res.*, *111*, B05305, doi:10.1029/2004JB003270.

Bréger, L., and B. Romanowicz (1998), Thermal and chemical 3D heterogeneity in D″, *Science*, *282*, 718–720.

Burke, K., B. Steinberger, T. H. Torsvik, and M. A. Smethurst (2008), Plume Generation Zones at the margins of Large Low Shear Velocity Provinces on the core-mantle boundary, *Earth Planet. Sci. Lett.*, *265*, 49–60, doi:10.1016/j.epsl.2007.09.042.

Choy, G. L., and P. Richards (1975), Pulse distortion and Hilbert transformation in multiply reflected and refracted body waves, *Bull. Seismol. Soc. Am.*, *65*, 55–70.

Dziewonski, A. M., and D. L. Anderson (1981), Preliminary reference Earth model, *Phys. Earth Planet. Inter.*, *25*, 297–356, doi:10.1016/0031-9201(81)90046-7.

Ford, S. R., E. D. Garnero, and A. K. McNamara (2006), A strong lateral shear velocity gradient and anisotropy heterogeneity in the lowermost mantle beneath the southern Pacific, *J. Geophys. Res.*, *111*, B03306, doi:10.1029/2004JB003574.

Garnero, E. J., and D. V. Helmberger (1996), Seismic detection of a thin laterally varying boundary layer at the base of the mantle beneath the central-Pacific, *Geophys. Res. Lett.*, *23*, 977–980, doi:10.1029/95GL03603.

Grand, S. P. (2002), Mantle shear-wave tomography and the fate of subducted slabs, *Philos. Trans. R. Soc. London A*, *360*, 2475–2491, doi:10.1098/rsta.2002.1077.

He, Y., and L. Wen (2009), Structural features and shear-velocity structure of the "Pacific Anomaly," *J. Geophys. Res.*, *114*, B02309, doi:10.1029/2008JB005814.

He, Y., L. Wen, and T. Zheng (2006), Geographic boundary and shear wave velocity structure of the Pacific anomaly near the core mantle boundary beneath the western Pacific, *Earth Planet. Sci. Lett.*, *244*, 302–314, doi:10.1016/j.epsl.2006.02.007.

Houser, C., G. Masters, P. Shearer, and G. Laske (2008), Shear and compressional velocity models of the mantle from cluster analysis of long-period waveforms, *Geophys. J. Int.*, *174*, 195–212, doi:10.1111/j.1365-246X.2008.03763.x.

Ishii, M., and J. Tromp (1999), Normal-mode and free-air gravity constraints on lateral variations in velocity and density of the Earth's mantle, *Science*, *285*, 1231–1236, doi:10.1126/science.285.5431.1231.

Kustowski, B., G. Ekström, and A. M. Dziwoński (2008), Anisotropic shear-wave velocity structure of the Earth's mantle: A global model, *J. Geophys. Res.*, *113*, B06306, doi:10.1029/2007JB005169.

Lay, T. (2006), A post-perovskite lens and D″ heat flux beneath the central Pacific, *Science*, *314*, 1272–1276, doi:10.1126/science.1133280.

Mao, W. L., H. Mao, W. Sturhahn, J. Zhao, V. B. Prakapenka, Y. Meng, J. Shu, Y. Fei, and R. J. Hemley (2006), Iron-rich post-Perovskite and the origin of ultralow-velocity zones, *Science*, *312*, 564–565, doi:10.1126/science.1123442.

Masters, G., G. Laske, H. Bolton, and A. M. Dziewonski (2000), The relative behavior of shear velocity, bulk sound speed, and compressional velocity in the mantle: Implications for chemical and thermal structure, in *Earth's Deep Interior: Mineral Physics and Tomography From the Atomic to the Global Scale*, *Geophys. Monogr. Ser.*, vol. 117, edited by S. Karato et al., pp. 63–87, AGU, Washington, D. C., doi:10.1029/GM117p0063.

McNamara, A. K., and S. Zhong (2004), Thermochemical structures within a spherical mantle: Superplumes or piles?, *J. Geophys. Res.*, *109*, B07402, doi:10.1029/2003JB002847.

McNamara, A. K., and S. Zhong (2005), Thermochemical structures beneath Africa and the Pacific ocean, *Nature*, *437*, 1136–1139, doi:10.1038/nature04066.

McNamara, A. K., E. J. Garnero, and S. Rost (2010), Tracking deep mantle reservoirs with ultra-low velocity zones, *Earth Planet. Sci. Lett.*, *299*, 1–9, doi:10.1016/j.epsl.2010.07.042.

Mégnin, C., and B. Romanowicz (2000), The shear velocity structure of the mantle from the inversion of body, surface, and higher modes waveforms, *Geophys. J. Int.*, *143*, 709–728, doi:10.1046/j.1365-246X.2000.00298.x.

Mori, J., and D. V. Helmberger (1995), Localized boundary layer below the mid-Pacific velocity anomaly identified from a PcP precursor, *J. Geophys. Res.*, *100*, 20,359–20,365, doi:10.1029/95JB02243.

Ni, S., and D. V. Helmberger (2003), Ridge-like lower mantle structure beneath South Africa, *J. Geophys. Res.*, *108*(B2), 2094, doi:10.1029/2001JB001545.

Ni, S., D. V. Helmberger, and J. Tromp (2005), Three-dimensional structure of the African superplume from waveform modelling, *Geophys. J. Int.*, *161*, 283–294, doi:10.1111/j.1365-246X.2005.02508.x.

Ohta, K., K. Hirose, T. Lay, N. Sata, and Y. Ohishi (2008), Phase transitions in pyrolite and MORB at lowermost mantle conditions: Implications for a MORB-rich pile above the core-mantle boundary, *Earth Planet. Sci. Lett.*, *267*, 107–117, doi:10.1016/j.epsl.2007.11.037.

Panning, M. P., V. Lekic, and B. A. Romanowicz (2010), The importance of crustal corrections in the development of a new global model of radial anisotropy, *J. Geophys. Res.*, *115*, B12325, doi:10.1029/2010JB007520.

Ritsema, J., A. Duess, H. J. van Heijst, and J. H. Woodhouse (2011), S40RTS: A degree-40 shear-velocity model for the mantle from new Rayleigh wave dispersion, teleseismic traveltime and normal-mode splitting function measurements, *Geophys. J. Int.*, *184*, 1223–1236, doi:10.1111/j.1365-246X.2010.04884.x.

Romanowicz, B. (2001), Can we resolve 3D density heterogeneity in the lower mantle?, *Geophys. Res. Lett.*, *28*, 1107–1110, doi:10.1029/2000GL012278.

Rost, S., and J. Revenaugh (2003), Small-scale ultralow-velocity zone structure imaged by *ScP*, *J. Geophys. Res.*, *108*(B1), 2056, doi:10.1029/2001JB001627.

Rost, S., E. J. Garnero, Q. Williams, and M. Manga (2005), Seismological constraints on a possible plume root at the core-mantle boundary, *Nature*, *435*, 666–669, doi:10.1038/nature03620.

Russell, S. A., C. Reasoner, T. Lay, and J. Revenaugh (2001), Coexisting shear- and compressional-wave seismic velocity discontinuities beneath the central Pacific, *Geophys. Res. Lett.*, *28*, 2281–2284, doi:10.1029/2000GL012553.

Schubert, G., G. Masters, P. Olson, and P. Tackley (2004), Superplumes or plume clusters?, *Phys. Earth Planet. Inter.*, *146*, 147–162, doi:10.1016/j.pepi.2003.09.025.

Simmons, N. A., A. M. Forte, L. Boschi, and S. P. Grand (2010), GyPSuM: A joint tomographic model of mantle density and seismic wave speeds, *J. Geophys. Res.*, *115*, B12310, doi:10.1029/2010JB007631.

Sun, D., D. Helmberger, S. Ni, and D. Bower (2009), Direct measures of lateral velocity variation in the deep mantle, *J. Geophys. Res.*, *114*, B05303, doi:10.1029/2008JB005873.

Tan, E., and M. Gurnis (2007), Compressible thermochemical convection and application to lower mantle structures, *J. Geophys. Res.*, *112*, B06304, doi:10.1029/2006JB004505.

Thorne, M. S., and E. J. Garnero (2004), Inferences on ultralow-velocity zone structure from a global analysis of SPdKS waves, *J. Geophys. Res.*, *109*, B08301, doi:10.1029/2004JB003010.

To, A., and B. Romanowicz (2009), Finite frequency effects on global S diffracted traveltimes, *Geophys. J. Int.*, *179*, 1645–1657, doi:10.1111/j.1365-246X.2009.04359.x.

To, A., B. Romanowicz, Y. Capdeville, and N. Takeuchi (2005), 3D effects of sharp boundaries at the borders of the African and Pacific superplumes: Observations and modeling, *Earth Planet. Sci. Lett.*, *233*, 137–153, doi:10.1016/j.epsl.2005.01.037.

Torsvik, T. H., M. A. Smethurst, K. Burke, and B. Steinberger (2006), Large igneous provinces generated from the margins of the large low-velocity provinces in the deep mantle, *Geophys. J. Int.*, *167*, 1447–1460, doi:10.1111/j.1365-246X.2006.03158.x.

Trampert, J., F. Deschamps, J. Resovsky, and D. Yuen (2004), Probabilistic tomography maps chemical heterogeneities throughout the lower mantle, *Science*, *306*, 853–856, doi:10.1126/science.1101996.

Vidale, J. E., and M. A. H. Hedlin (1998), Evidence for partial melt at the core-mantle boundary north of Tonga from the strong scattering of seismic waves, *Nature*, *391*, 682–685, doi:10.1038/35601.

Wang, Y., and L. Wen (2004), Mapping the geometry and geographic distribution of a very low velocity province at the base of the Earth's mantle, *J. Geophys. Res.*, *109*, B10305, doi:10.1029/2003JB002674.

Wang, Y., and L. Wen (2007), Geometry and P and S velocity structure of the "African Anomaly," *J. Geophys. Res.*, *112*, B05313, doi:10.1029/2006JB004483.

Wen, L. (2001), Seismic evidence for a rapidly varying compositional anomaly at the base of the Earth's mantle beneath the Indian Ocean, *Earth Planet. Sci. Lett.*, *194*, 83–95, doi:10.1016/S0012-821X(01)00550-7.

Wen, L. (2002), An SH hybrid method and shear velocity structures in the lowermost mantle beneath the central Pacific and South Atlantic Oceans, *J. Geophys. Res.*, *107*(B3), 2055, doi:10.1029/2001JB000499.

Wen, L. (2006), A compositional anomaly at the Earth's core-mantle boundary as an anchor to the relatively slowly moving surface hotspots and as source to the DUPAL anomaly, *Earth Planet. Sci. Lett.*, *246*, 138–148, doi:10.1016/j.epsl.2006.04.024.

Wen, L., and D. L. Anderson (1995), The fate of slabs inferred from seismic tomography and 130 million years of subduction, *Earth Planet. Sci. Lett.*, *133*, 185–198, doi:10.1016/0012-821X(95)00064-J.

Wen, L., and D. V. Helmberger (1998a), Ultra-low velocity zones near the core-mantle boundary from broadband PKP precursors, *Science*, *279*, 1701–1703, doi:10.1126/science.279.5357.1701.

Wen, L., and D. V. Helmberger (1998b), A two-dimensional P-SV hybrid method and its application to modeling localized structures near the core-mantle boundary, *J. Geophys. Res.*, *103*, 17,901–17,918, doi:10.1029/98JB01276.
Wen, L., P. Silver, D. James, and R. Kuehnel (2001), Seismic evidence for a thermo-chemical boundary at the base of the Earth's mantle, *Earth Planet. Sci. Lett.*, *189*, 141–153, doi:10.1016/S0012-821X(01)00365-X.
Wessel, P., and W. H. F. Smith (1995), New version of the generic mapping tools, *Eos Trans. AGU*, *76*(33), 329, doi:10.1029/95EO00198.
Wicks, J. K., J. M. Jackson, and W. Sturhahn (2010), Very low sound velocities in iron-rich (Mg, Fe)O: Implications for the core-mantle boundary region, *Geophys. Res. Lett.*, *37*, L15304, doi:10.1029/2010GL043689.